

# High-pressure synthesis of ultraincompressible hard rhenium nitride pernitride $\text{Re}_2(\text{N}_2)\text{N}_2$ stable at ambient conditions

Maxim Bykov<sup>1,\*</sup>, Stella Chariton<sup>1</sup>, Hongzhan Fei<sup>1</sup>, Timofey Fedotenko<sup>2</sup>, Georgios Aprilis<sup>2</sup>, Alena V. Ponomareva<sup>3</sup>, Ferenc Tasnádi<sup>4</sup>, Igor A. Abrikosov<sup>4</sup>, Benoit Merle<sup>5</sup>, Patrick Feldner<sup>5</sup>, Sebastian Vogel<sup>6</sup>, Wolfgang Schnick<sup>6</sup>, Vitali B. Prakapenka<sup>7</sup>, Eran Greenberg<sup>7</sup>, Michael Hanfland<sup>8</sup>, Anna Pakhomova<sup>9</sup>, Hanns-Peter Liermann<sup>9</sup>, Tomoo Katsura<sup>1</sup>, Natalia Dubrovinskaia<sup>2</sup>, Leonid Dubrovinsky<sup>1</sup>

<sup>1</sup>Bayerisches Geoinstitut, University of Bayreuth, Universitätsstraße 30, 95440 Bayreuth, Germany

<sup>2</sup>Material Physics and Technology at Extreme Conditions, Laboratory of Crystallography, University of Bayreuth, 95440 Bayreuth, Germany

<sup>3</sup>Materials Modeling and Development Laboratory, National University of Science and Technology 'MISIS', Moscow 119049, Russia

<sup>4</sup>Department of Physics, Chemistry and Biology (IFM), Linköping University, SE-58183 Linköping, Sweden

<sup>5</sup>Materials Science & Engineering, Institute I, Friedrich-Alexander-Universität Erlangen-Nürnberg (FAU) Martensstraße. 5, D-91058 Erlangen, Germany

<sup>6</sup>Chair in Inorganic Solid State Chemistry, Department of Chemistry University of Munich (LMU), Butenandtstraße 5-13 (D), D-81377 Munich (Germany)

<sup>7</sup>Center for Advanced Radiation Sources, University of Chicago, 9700 South Cass Avenue, Argonne, IL 60437, USA

<sup>8</sup>European Synchrotron Radiation Facility, BP 220, 38043 Grenoble Cedex, France

<sup>9</sup>Photon Science, Deutsches Elektronen-Synchrotron, Notkestraße 85, 22607 Hamburg, Germany.

\*E-mail: [maks.byk@gmail.com](mailto:maks.byk@gmail.com)

**Keywords:** incompressible materials, superhard, nitrides, high-pressure

**High-pressure synthesis can yield unique compounds with advanced properties, but usually they are either unrecoverable at ambient conditions or produced in quantity insufficient for properties characterization<sup>1-4</sup>. Here we report the synthesis of metallic, ultraincompressible (bulk modulus  $K_0 = 428(10)$  GPa), and very hard (nanoindentation hardness  $36.7(8)$  GPa) rhenium (V) nitride pernitride  $\text{Re}_2(\text{N}_2)\text{N}_2$ . First it was obtained through a direct reaction between rhenium and nitrogen at 40 to 90 GPa in a laser-heated diamond anvil cell. The synthesis was scaled up through a reaction between rhenium and ammonium azide in a large-volume press at 33 GPa. Although metallic bonding is typically seen incompatible with intrinsic hardness,  $\text{Re}_2(\text{N}_2)\text{N}_2$  turned to be at a threshold for superhard materials. Our work demonstrates a feasibility of surmounting conceptions common in material sciences.**

According to the approach formulated by Yeung *et al.*<sup>4</sup>, the design of novel superhard materials should be based on the combination of a metal with high valence electron density with the first-row main-group elements, which form short covalent bonds to prevent dislocations. This conclusion was based on the synthesis of hard borides, such as  $\text{OsB}_2$ <sup>5</sup>,  $\text{ReB}_2$ <sup>6-8</sup>,  $\text{FeB}_4$ <sup>9</sup> or  $\text{WB}_4$ <sup>10</sup>, whose crystal structures possess covalently bonded boron networks. Similar to boron, nitrogen as well can form covalent nitrogen-nitrogen bonds, but there are several factors, which make it difficult to synthesize nitrogen-rich nitrides. The large bond enthalpy of the triply bound  $\text{N}_2$  molecule ( $941 \text{ kJ}\cdot\text{mol}^{-1}$ )<sup>11</sup> makes this element generally unreactive. In many reactions the activation barrier for  $\text{N}_2$  bond breaking requires temperatures, which are higher than the decomposition temperatures of the target phases.  $\text{MN}_x$  compounds with  $x > 1$  are rarely available *via* direct nitridation reactions or ammonothermal syntheses<sup>12,13</sup>. Therefore, binary systems  $M$ - $\text{N}$  systems are often limited to interstitial metal-rich nitrides. Usually, they are less compressible and have higher bulk moduli in comparison with pure metals due to the increasing repulsion between metal and nitrogen atoms, whereas their shear moduli are not always much different from those of metals.

Application of pressure is one way to increase the chemical potential of nitrogen and to stabilize nitrogen-rich phases.<sup>14</sup> Several transition metal dinitrides,  $\text{PtN}_2$ <sup>15</sup>,  $\text{PdN}_2$ <sup>16</sup>,  $\text{IrN}_2$ <sup>17</sup>,  $\text{OsN}_2$ <sup>17</sup>,  $\text{TiN}_2$ <sup>18</sup>,  $\text{RhN}_2$ <sup>19</sup>,  $\text{RuN}_2$ <sup>20</sup>,  $\text{CoN}_2$ <sup>21</sup> and  $\text{FeN}_2$ <sup>22</sup>, containing covalently bound dinitrogen units were recently synthesized in laser-heated diamond anvil cells (LHDACs) *via* reactions between elemental metal and nitrogen in a pressure range of 40-80 GPa. Although LHDAC is an efficient method to study high-pressure chemical reactions, it is challenging to scale up the synthesis. The search for suitable synthetic strategies, which would enable an appropriate

reaction to be realized in a large volume press (LVP) instead of a LHDAC, is an important challenge for high-pressure chemistry and materials sciences. In this study, focusing on the high-pressure synthesis of novel nitrogen-rich phases in the Re-N system and the development of new synthetic strategies, we resolved this problem for a previously unknown rhenium nitride  $\text{ReN}_2$  with unusual crystal chemistry and unique properties.

Direct reactions between rhenium and nitrogen were studied by Friedrich *et al.*<sup>23</sup>, who synthesized two interstitial rhenium nitrides  $\text{Re}_3\text{N}$  at 13 GPa and 1700 K, and  $\text{Re}_2\text{N}$  at 20 GPa and 2000 K. Both compounds have exceptionally large bulk moduli exceeding 400 GPa (as measured upon compression in a non-hydrostatic medium<sup>23</sup>), but only moderate shear moduli as expected for interstitial compounds<sup>24</sup>. Kawamura *et al.*<sup>25</sup> reported synthesis of  $\text{ReN}_2$  with  $\text{MoS}_2$  structure type (*m*- $\text{ReN}_2$ ) in a metathesis reaction between  $\text{Li}_3\text{N}$  and  $\text{ReCl}_5$  at 7.7 GPa. Subsequently, Wang *et al.*<sup>26</sup> suggested, based on the first-principle calculations, that *m*- $\text{ReN}_2$  is unstable and ‘real stoichiometric’  $\text{ReN}_2$  should have monoclinic *C2/m* symmetry and transform to the tetragonal *P4/mbm* phase above 130 GPa. However, this suggestion has not been proven experimentally as yet. Recently Bykov *et al.* reported a novel inclusion polynitrogen compound  $\text{ReN}_8 \cdot x\text{N}_2$  synthesized from elements at 106 GPa<sup>27</sup>, but the region of ~35-100 GPa still remains completely unexplored for the Re-N system.

To fill this gap in pressure and temperature space, we have studied chemical reactions between Re and nitrogen and other reagents, such as sodium azide  $\text{NaN}_3$  and ammonium azide  $\text{NH}_4\text{N}_3$ , in LHDACs in a range of 26 – 87 GPa at temperatures of 2000 – 2500 K (Table 1, Experiments #1 through #6). The reactions products typically contained numerous single-crystalline grains of several rhenium nitride phases (Table 1), which were identified using synchrotron single-crystal X-ray diffraction (Supplementary Figure 1, Supplementary Table 1).

**Table 1. Summary of syntheses**

Experiment,	Technique	Reagents	Pressure (GPa)	Temperature (K)	Products
1	LHDAC	Re + $\text{N}_2$	42	2200(300)	$\text{ReN}_2 + \text{Re}_2\text{N} + \text{ReN}_{0.6}$
2	LHDAC	Re + $\text{N}_2$	49	2200(300)	$\text{ReN}_2 + \text{Re}_2\text{N}$
3	LHDAC	Re + $\text{N}_2$	71	2500(300)	$\text{ReN}_2 + \text{Re}_2\text{N}$
4	LHDAC	Re + $\text{N}_2$	86	2400(300)	$\text{ReN}_2 + \text{Re}_2\text{N}$
5	LHDAC	Re + $\text{NaN}_3$	29	2000(300)	$\text{NaReN}_2 + \text{Re}_2\text{N}$
6	LHDAC	Re + $\text{NH}_4\text{N}_3$	43	2200(300)	$\text{ReN}_2 + \text{ReN}_{0.6} + \text{Re}_2\text{N}$
7	LVP	Re + $\text{NH}_4\text{N}_3$	33	2273(100)	$\text{ReN}_2 + \text{Re}_2\text{N}$

A direct reaction between Re and  $\text{N}_2$  (Table 1) resulted in the synthesis of three rhenium nitrides  $\text{ReN}_2$ ,  $\text{Re}_2\text{N}$ , and  $\text{ReN}_{0.6}$ , two of which ( $\text{ReN}_2$  and  $\text{ReN}_{0.6}$ ) have never been observed before. The third phase identified in these experiments,  $\text{Re}_2\text{N}$  (*P6<sub>3</sub>/mmc*), has previously been reported<sup>23</sup>. After a stepwise decompression of the sample obtained in Experiment #1 down to

the ambient pressure, all of the three phases ( $\text{ReN}_2$ ,  $\text{ReN}_{0.6}$ ,  $\text{Re}_2\text{N}$ ) were found to remain intact even after one month (Supplementary Figure 4). Crystal structure analysis of  $\text{ReN}_{0.6}$  showed that it has a defect WC structure type (space group  $P\bar{6}m2$ ) (for details on  $\text{ReN}_{0.6}$  see Supplementary Information; Supplementary Figures 2, 3, Supplementary Table 2).

Analysis of the crystal structure of  $\text{ReN}_2$  revealed its unusual crystal-chemistry. Figure 1 shows the crystal structure of  $\text{ReN}_2$ , which is built of distorted  $\text{ReN}_7$  capped trigonal prisms (Figure 1d) and contains both N-N units (dumbbells) (Figure 1f) and discrete N atoms (N2) (Figure 1e) in an atomic ratio 1:1. The N1-N1 dumbbells are located in a trigonal antiprism formed by Re atoms (Figure 1f), while discrete N2 atoms have a tetrahedral coordination by Re (Figure 1e). The N1-N1 bond length ( $d_{\text{N1-N1}} = 1.412(16)$  Å at ambient conditions) suggests that the  $\text{N}_2$  unit should be considered as a pernitride anion  $\text{N}_2^{4-}$ . Therefore,  $\text{ReN}_2$  is a rhenium nitride pernitride and its crystal-chemical formula is  $\text{Re}^{+\text{V}}_2[\text{N}^{\text{II}}_2][\text{N}^{\text{III}}]_2$ .

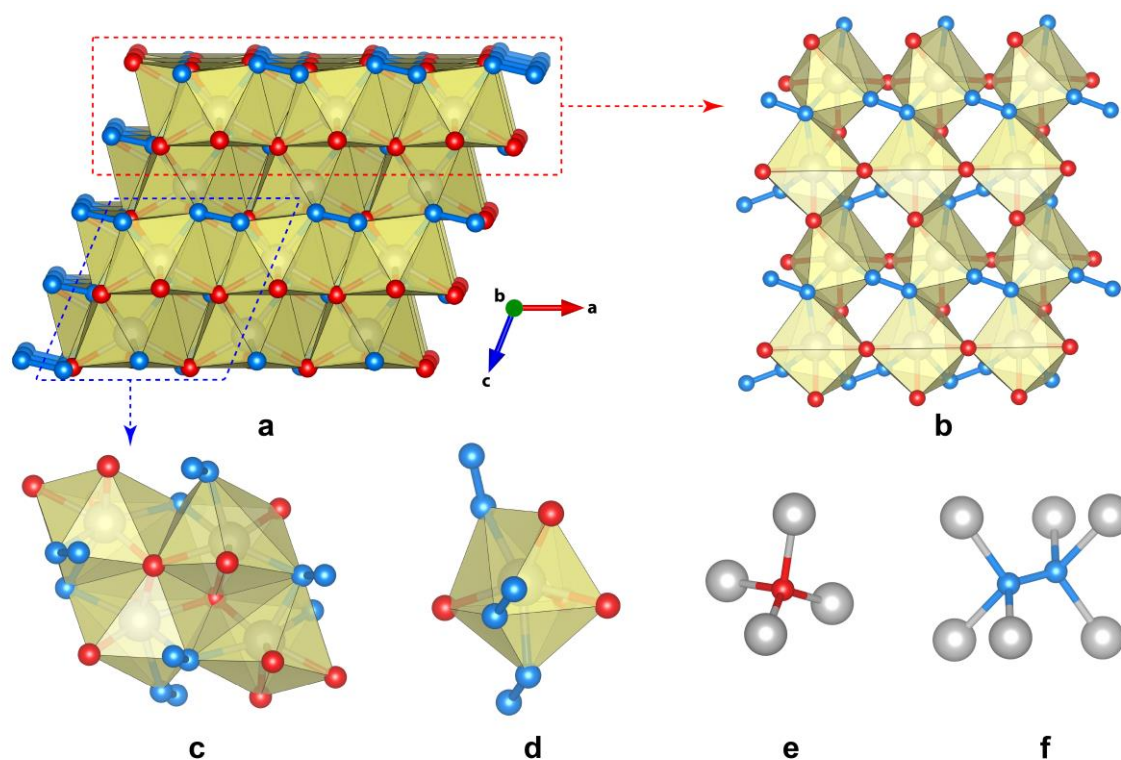


**Figure 1. Fragments of the crystal structure of  $\text{Re}_2(\text{N}_2)(\text{N})_2$  at ambient conditions. Re atoms – gray, N1 atoms – blue, N2 atoms – red.**  $\text{ReN}_2$  crystallizes in the space group  $P2_1/c$  (No. 14) with  $a = 3.6254(17)$ ,  $b = 6.407(7)$ ,  $c = 4.948(3)$  Å,  $\beta = 111.48(6)^\circ$ . Rhenium and nitrogen atoms occupy crystallographic sites  $4e$ : Re [0.35490(11), 0.34041(8), 0.19965(8)], N1 [0.194(2), 0.038(2), 0.311(19)], N2 [0.259(3), 0.6381(18), 0.024(2)]. Full crystallographic information is given in the supplementary crystallographic information file and in the Supplementary Tables 3 and 4. (a) The projection of the crystal structure along the  $b$ -axis. (b,c) Fragments of the crystal structure of  $\text{ReN}_2$  showing how  $\text{ReN}_7$  polyhedra are connected with each other. (d) Separate  $\text{ReN}_7$  coordination polyhedron. (e) Coordination of N2 atoms. (f) Coordination of N1-N1 dumbbells.

The compressibility of  $\text{ReN}_2$  was measured on the sample #2 (Table 1), which was synthesized at 49 GPa, then decompressed down to ambient conditions, and re-loaded into another DAC with a neon pressure-transmitting medium, which provides much better hydrostaticity of the sample environment than nitrogen<sup>28</sup>. The sample was first characterized using single-crystal XRD at ambient conditions. On compression, the lattice parameters were extracted from the powder XRD data (Figure 2*a,b*; Supplementary Figures 4-6; Supplementary Table 5). The pressure-volume dependence was described using the third-order Birch-Murnaghan equation of state<sup>29</sup> with the following fit parameters:  $V_0 = 107.21(4) \text{ \AA}^3$ ,  $K_0 = 428(10) \text{ GPa}$ ,  $K' = 1.6(5)$ . Figure 2*c* shows a plot of correlated values of  $K_0$  and  $K'$  to different confidence levels. The bulk modulus  $K_0$  lies within the range of 410-447 GPa at the 99.73% confidence level. Thus,  $K_0$  of  $\text{ReN}_2$  is larger than that of any compound in the Re-N system and is comparable to that of diamond ( $K_0 = 440 \text{ GPa}$ ) and  $\text{IrN}_2$  ( $K_0 = 428(12) \text{ GPa}$ )<sup>17</sup>. Among very incompressible pernitrides of transition metals,  $\text{ReN}_2$  is the only compound, in which the metal atom has oxidation state (+V) higher than (+IV). The increased ionicity of Re-N chemical bonding, compared to those in other pernitrides may, therefore, play a role in the enhancement of the bulk modulus of  $\text{ReN}_2$  in comparison to  $\text{OsN}_2$ ,  $\text{PtN}_2$  and  $\text{TiN}_2$ . This is in agreement with the trend recently proposed by Bykov *et al.*<sup>22</sup>, who showed that the bulk moduli of dinitrides  $\text{MN}_2$  increase with the increase of the oxidation state of metal atoms from +II to +IV.

More detail characterization of physical properties of  $\text{ReN}_2$ , such as hardness, electrical conductivity *etc.* require a sample to be at least a few tens of microns in size that is much larger than can be synthesized in a LHDAC. The large volume press technique enables the synthesis of such a sample, but precludes from using  $\text{N}_2$  as a reagent. First, the amount of nitrogen, which can be sealed in a capsule along with Re, is insufficient for the desired reaction yield; second, unavoidable deformation of the capsule upon compression may potentially lead to the loss of nitrogen. Therefore, a solid source of nitrogen had to be found and we tested sodium and ammonium azides,  $\text{NaN}_3$  and  $\text{NH}_4\text{N}_3$ , as potential precursors in LHDACs (Experiments #5, #6, Table 1) (for a discussion regarding the choice of the solid reagents see Supplementary Information). The experiment with  $\text{NaN}_3$  (Experiment #5) did not result in the synthesis of  $\text{ReN}_2$ . The major product of the reaction was  $\text{NaReN}_2$  (Supplementary Figure 7), whose lattice parameters turned out to be very close to those reported for *m*- $\text{ReN}_2$  by Kawamura *et al.*<sup>25</sup>, that might suggest that the material described in Ref. 25 as rhenium nitride indeed could be a different compound (for a related discussion see Supplementary Information). The experiment in LHDAC with  $\text{NH}_4\text{N}_3$  as a source of nitrogen resulted in the synthesis of  $\text{ReN}_2$  among other products (Experiment #6, Table 1).

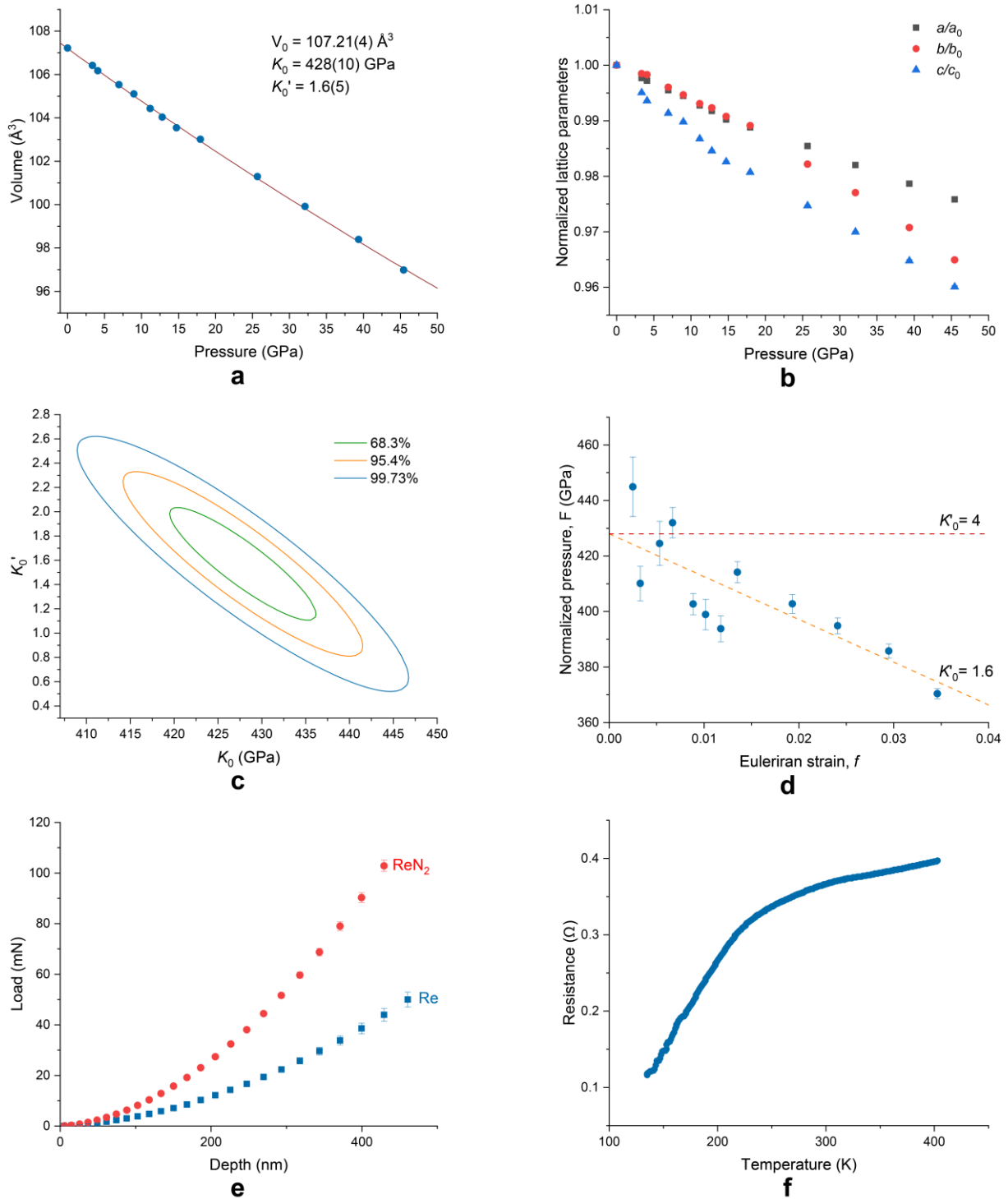


**Figure 2. Physical properties of  $\text{Re}_2(\text{N}_2)\text{N}_2$**  (a) Pressure-dependence of the unit-cell volume and (b) normalized lattice parameters of  $\text{ReN}_2$ . (c) Plot of the correlated values of  $K_0$  and  $K_0'$  to different confidence levels of 68.3%, 95.4% and 99.73%, respectively. (d) An  $F$ - $f$  plot based on Birch-Murnaghan EoS. (e) Averaged indentation load-displacement data. The error bars correspond to the standard deviation between 16 single measurements at different locations. (f) Temperature dependence of the electrical resistance of the  $\text{ReN}_2$  sample at ambient pressure.

Based on results of this experiment in DAC, we explored a possibility to scale up the synthesis of  $\text{ReN}_2$  in a multianvil LVP at 33 GPa and 2273 K via a reaction between rhenium and ammonium azide (Experiment #7, Supplementary Figure 8). The product of the reaction was a mixture of  $\text{Re}_2\text{N}$  and  $\text{ReN}_2$ . Each phase was separated (Supplementary Figure 9) and characterized using single-crystal X-ray diffraction. A phase-pure polycrystalline sample of  $\text{ReN}_2$  ( $70 \times 60 \times 50 \mu\text{m}^3$ ), which was synthesized in the LVP, was used for nanoindentation hardness and electrical resistance measurements. Nanoindentation was performed using a nanoindenter equipped with Berkovich diamond tip and featuring continuous stiffness measurement capabilities. The average hardness and Young's modulus measured between 200 and 400 nm depths are 36.7(8) GPa and 493(14) GPa respectively (Figure 2e, Table 3). The hardness approaching 40 GPa, a threshold for superhard materials, and extreme stiffness comparable with diamond makes mechanical properties of  $\text{ReN}_2$  exceptional in the row of metal nitrides. Due to the directional N-N bonding, the hardness of  $\text{ReN}_2$  is higher than that of known interstitial transition metal nitrides ( $\delta\text{-NbN}$  – 20 GPa,  $\text{HfN}$  – 19.5 GPa,  $\text{ZrN}$  – 17.4 GPa<sup>30</sup>,  $\text{CrN}$  – 17 GPa<sup>4</sup> *etc.*). Most transition metal pernitrides  $\text{MN}_2$  that are metastable at ambient conditions are expected to be very hard compounds too, however they were never obtained in a quantity sufficient for the hardness measurements<sup>31,32</sup>.

The electrical resistance of  $\text{ReN}_2$  as a function of temperature was measured at ambient pressure on a sample with the dimensions of about  $70 \times 60 \times 50 \mu\text{m}^3$ . The results of the measurements in the range of 150 K to 400 K are shown in Figure 2f. Electrical resistivity of metals increases with temperature and this is the case for  $\text{ReN}_2$ . The shape of the resistance – temperature curve (Figure 2f) is reproducible as confirmed in a number of independent measurements on the same sample with re-glued electrical contacts.

To confirm the experimentally observed peculiarities of  $\text{ReN}_2$  and to gain deeper insights into the mechanical and electronic properties of this compound, we performed theoretical calculations based on the density functional theory. First, we considered the crystal structure of  $\text{ReN}_2$ . We carried out the full structure optimization for the compound at ambient pressure and found that calculations and experiment are in very close agreement (Supplementary Table 3). Calculated elastic constants for  $\text{ReN}_2$  (Table 2) fulfill the mechanical stability conditions<sup>33</sup>, and calculated phonon dispersion relations (Figure 3a) show only real frequencies confirming its dynamic stability. Theoretically calculated N1–N1 vibrational frequency form a localized band giving rise to a peak of the phonon density of states at  $\sim 1031 \text{ cm}^{-1}$ . This vibrational behavior is similar to other pernitrides<sup>15,18,34</sup>. The metallic nature of the material confirmed by our calculations of the electronic density of states (DOS) (Figure 3c).

Calculated vibrational and electronic properties of N1-N1 unit confirm that it is a pernitride anion  $N_2^{4-}$ . On the contrary, electronic and vibrational properties of N2 atoms (Figure 3a,c) are quite distinct from those of N1, providing strong support to the experimental observation of the crystal chemistry of  $ReN_2$ , which is unique for transition metals pernitrides.

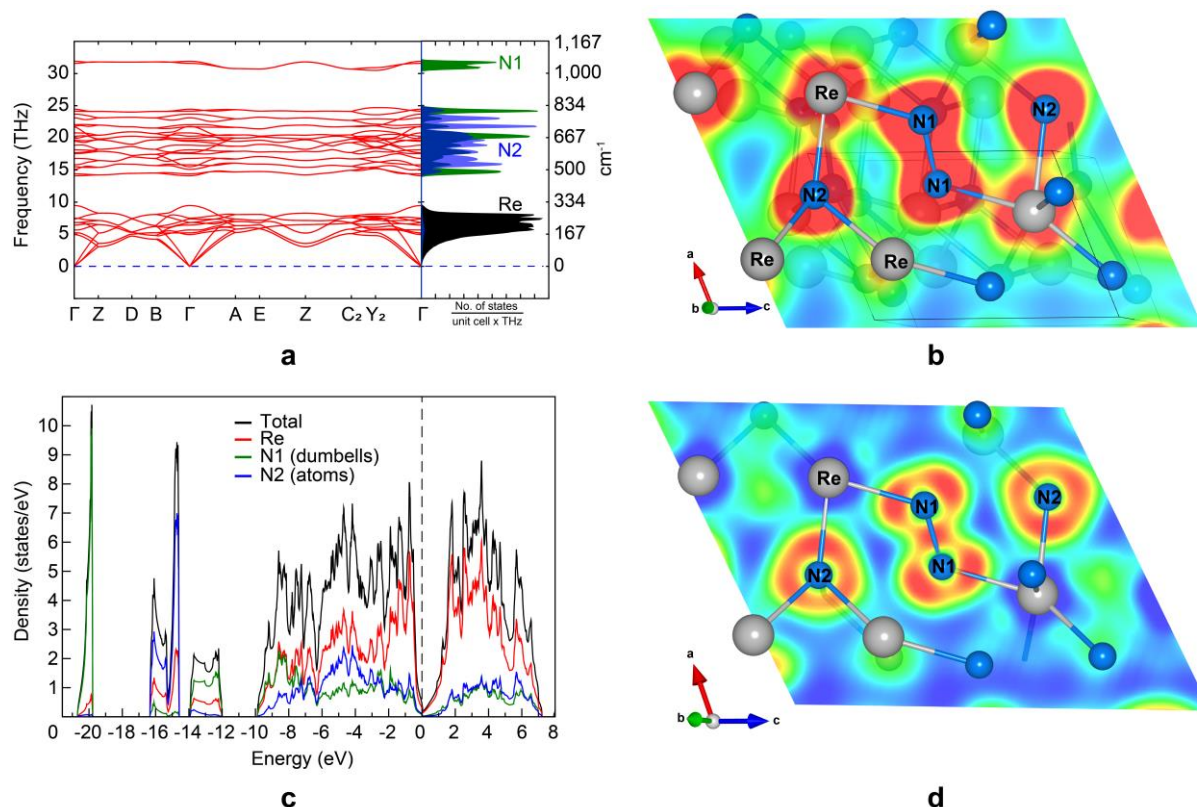


**Figure 3. Phonon and electronic structure calculations for  $ReN_2$ .** Calculated phonon dispersion relations (a), charge density map (b), densities of states (c) and electron localization function (d) for  $ReN_2$  at ambient conditions.

The unique chemistry of the compound is essential for understanding its superior mechanical properties. The bulk modulus, calculated theoretically using Voigt-Reuss-Hill approximation (413.5 GPa)<sup>35</sup> is in a good agreement with the experiment (428(10) GPa), confirming that  $ReN_2$  can be characterized as highly incompressible material. At the same time, the value of the Poisson coefficient is close to 0.25, and relatively high ratio between shear and bulk elastic moduli indicates substantial degree of covalence in  $ReN_2$  chemical bonding. A direct calculation of the charge density map (Figure 3b) confirms the expectation. One sees a formation of covalent bonds between two N1 atoms. It is of single bond character with very high degree of electron localization (Figure 3d) typical for a pernitride anion  $N_2^{4-}$  in other transition metal pernitrides,<sup>36</sup> and incompressible  $N_2^{4-}$  is supposed to contribute to very low compressibility of the materials. The covalent bond between Re and N2 atoms is formed by



substantially less localized electrons (compare Fig. 3b and Fig 3d). Indeed, measured temperature dependence of the electrical resistance (Figure 2f) and the estimated resistivity ( $\sim 4 \cdot 10^{-6} \Omega \cdot \text{m} - 16 \cdot 10^{-6} \Omega \cdot \text{m}$  in a temperature range 150-400 K) are in agreement with the theoretical conclusion and the description of  $\text{ReN}_2$  as a metal. The formation of the covalent bonds between Re and N2 atoms indicates strong hybridization between the electronic states of the atoms. The calculated electronic DOS (Figure 3c) shows the presence of the pseudogap between occupied, predominantly bonding states of Re and unoccupied non-bonding and anti-bonding states. According to S.-H. Jhi *et al.*<sup>37</sup>, such features optimize electronic contribution to hardness enhancement in transition-metal carbonitrides, which can also explain very high hardness of  $\text{ReN}_2$ . Thus, the formation of strong covalent bond between Re and N2 atoms, a unique feature of the material synthesized in this work in comparison with known transition metal pernitrides, appears to be essential for its spectacular mechanical and electronic properties.

**Table 2. Calculated elastic constants  $C_{ij}$  (GPa), bulk modulus  $B$  (GPa), shear modulus  $G$  (GPa), Young's modulus  $E$  (GPa) and Poisson's ratio ( $\nu$ ) of  $\text{ReN}_2$**

$C_{11}$	$C_{12}$	$C_{13}$	$C_{15}$	$C_{22}$	$C_{23}$	$C_{25}$	$C_{33}$	$C_{35}$
869.51	230.73	261.47	51.01	748.93	251.83	26.67	648.06	16.61
$C_{44}$	$C_{46}$	$C_{55}$	$C_{66}$	$B$	$G$	$E$	$\nu$	
257.43	35.91	299.94	266.34	413.5	262	650	0.24	

**Table 3. Mean hardness and Young's modulus measured by nanoindentation in the 200-400 nm depth range. The error estimate corresponds to the standard deviation between 16 different locations.**

Material	Hardness (GPa)	Young's modulus (GPa)
$\text{ReN}_2$	36.7(8)	493(14)
Re	10.9(6)	424(12)

To summarize, in the present work we have synthesized a novel transition metal nitride  $\text{ReN}_2$  ( $\text{Re}^{+\text{V}}_2(\text{N}^{\text{-II}})_2(\text{N}^{\text{-III}})_2$ ) with the unique crystal structure and outstanding properties. The structure with Re atoms in the high oxidation state +V features both discrete nitride and pernitride ions. A combination of the high electron density of the transition metal with interstitial nitride anions and covalently bound pernitride units makes this compound ultraincompressible and extremely hard at the same time. The developed method for scaling up

the synthesis of  $\text{ReN}_2$  in a LVP using ammonium azide as a nitrogen precursor may be applied for producing other transition metal nitrides. We demonstrated the complete route for materials development from screening experiments in diamond anvil cells to the synthesis of samples large enough for physical property measurements. It is not only our results *per se* that are important, but the fact that the development and synthesis of the new material was realized contrary to established concepts and should encourage further theoretical and experimental works in the field.

## Methods

### *Synthesis of Re-N phases in laser-heated diamond anvil cells*

In all synthesis experiments a rhenium powder (Sigma Aldrich, 99.995 %) was loaded into the sample chamber of a BX90 diamond anvil cell (Boehler-Almax anvils, 250- $\mu\text{m}$  size). In four experiments the chamber was filled with nitrogen at 1.5 kbar that served as a pressure-transmitting medium and as a reagent. In two experiments, the chamber was filled either with ammonium azide  $\text{NH}_4\text{N}_3$  or with sodium azide  $\text{NaN}_3$ . Pressure was determined using the equation of state of rhenium<sup>38–40</sup>. The compressed sample was heated using the double-sided laser-heating system installed at the Bayerisches Geoinstitut (BGI), University of Bayreuth, Germany. Successful syntheses were performed at 40, 42, 49, 71 and 86 GPa at temperatures of 2200–2500 K (Table 1).

### *Synthesis of Re-N phases in the large-volume press*

High-pressure synthesis was performed using a Kawai-type multi-anvil apparatus IRIS15, installed at the BGI<sup>41</sup>. The  $\text{NH}_4\text{N}_3$  sample (0.5 mm thickness, 0.8 mm in diameter) was sandwiched between two layers of Re powder (0.1 mm thick, 0.8 mm in diameter) and between two tubes of dense alumina in a Re capsule, which also acted as a heater. The capsule was placed in a 5 wt%  $\text{Cr}_2\text{O}_3$ -doped MgO octahedron with a 5.7 mm edge that was used as the pressure medium. The assembly scheme is given in the Supplementary Figure 11. Eight tungsten carbide cubes with 1.5 mm truncation edge lengths were used to generate high pressures. The assembly was pressurized at ambient temperature to 33 GPa, following the calibration given by Ishii *et al.*<sup>41</sup> and then heated to  $\sim 2273(100)$  K within 5 minutes and immediately quenched after the target temperature was reached. The assembly was then decompressed during 16 hours.

### *Synthesis of $\text{NH}_4\text{N}_3$*

Ammonium azide,  $\text{NH}_4\text{N}_3$  was obtained by the metathesis reaction between  $\text{NH}_4\text{NO}_3$  (2.666 g, 33mmol, Sigma-Aldrich, 99.0%) and  $\text{NaN}_3$  (2.165 g, 33 mmol, Acros Organics, Geel,

Belgium, 99%) in a Schlenk tube. By heating from room temperature to 170°C in a glass oven and annealing for 7.5 h at 170°C and then for 12h at 185°C, NH<sub>4</sub>N<sub>3</sub> precipitated at the cold end of the tube separated from NaNO<sub>3</sub>, which remained at the hot end during the reaction<sup>42</sup>.

#### *Compressibility measurements*

For the compressibility measurements the sample synthesized at 49 GPa and 2200 K (Experiment #2) was quenched down to ambient pressure and re-loaded into another diamond anvil cell. The sample chamber was then filled with Ne that served as a pressure-transmitting medium. A powder of gold (Sigma Aldrich, 99.99 %) was placed into the sample chamber along with the sample and used as a pressure standard<sup>43</sup>. The sample was then compressed up to ~45 GPa in 13 steps. At each pressure point we have collected powder X-ray diffraction data.

#### *Synchrotron X-ray diffraction*

High-pressure single-crystal and powder synchrotron X-ray diffraction studies of the reaction products were performed at the beamlines P02.2 (DESY, Hamburg, Germany)<sup>44</sup>, ID15B (ESRF, Grenoble, France) and GSECARS beamline (APS, Argonne, USA). The following beamline setups were used. P02.2:  $\lambda = 0.29 \text{ \AA}$ , beam size  $\sim 2 \times 2 \text{ \mu m}^2$ , Perkin Elmer XRD 1621 detector; ID15B:  $\lambda = 0.41$ , beam size  $\sim 10 \times 10 \text{ \mu m}^2$ , Mar555 flat panel detector; GSECARS:  $\lambda = 0.2952 \text{ \AA}$ , beam size  $\sim 3 \times 3 \text{ \mu m}^2$ , Pilatus CdTe 1M detector. For the single-crystal XRD measurements samples were rotated around a vertical  $\omega$ -axis in a range  $\pm 38^\circ$ . The diffraction images were collected with an angular step  $\Delta\omega = 0.5^\circ$  and an exposure time of 1s/frame. For analysis of the single-crystal diffraction data (indexing, data integration, frame scaling and absorption correction) we used the *CrysAlis<sup>Pro</sup>* software package. To calibrate an instrumental model in the *CrysAlis<sup>Pro</sup>* software, *i.e.*, the sample-to-detector distance, detector's origin, offsets of goniometer angles, and rotation of both X-ray beam and the detector around the instrument axis, we used a single crystal of orthoenstatite ((Mg<sub>1.93</sub>Fe<sub>0.06</sub>)(Si<sub>1.93</sub>, Al<sub>0.06</sub>)O<sub>6</sub>, *Pbca* space group,  $a = 8.8117(2)$ ,  $b = 5.18320(10)$ , and  $c = 18.2391(3) \text{ \AA}$ ). The same calibration crystal was used at all the beamlines.

Powder diffraction measurements were performed either without sample rotation (still images) or upon continuous rotation in the range  $\pm 20^\circ\omega$ . The images were integrated to powder patterns with Dioptas software<sup>45</sup>. Le-Bail fits of the diffraction patterns were performed with the TOPAS6 software.

#### *In-house X-ray diffraction*

Ambient-pressure single-crystal XRD datasets were collected with a high-brilliance Rigaku diffractometer (Ag *K* $\alpha$  radiation) equipped with Osmic focusing X-ray optics and Bruker Apex CCD detector in the BGI.

### *Structure solution and refinement*

The structure was solved with the ShelXT structure solution program<sup>46</sup> using intrinsic phasing and refined with the Jana 2006 program<sup>47</sup>. CSD-1897795 contains the supplementary crystallographic data for this paper. These data can be obtained free of charge from FIZ Karlsruhe via [www.ccdc.cam.ac.uk/structures](http://www.ccdc.cam.ac.uk/structures)

### *Nanoindentation*

Nanoindentation was performed using a Nanoindenter G200 platform (KLA-Tencor, Milpitas, CA, USA), equipped with a Berkovich diamond tip (Synton MDP, Nidau, Switzerland) and featuring the continuous stiffness based method (CSM)<sup>48</sup>. Each sample was indented at 16 different locations separated by a distance of at least 10  $\mu\text{m}$ , so that their plastic zones did not overlap. For each measurement, loading was performed at a constant strain-rate of  $0.025\text{ s}^{-1}$  up to a maximal indentation depth of at least 400 nm. A 2 nm large oscillation superimposed on the loading signal allowed continuously measuring the contact stiffness. The acquired data were evaluated using the Oliver-Pharr method<sup>49,50</sup>. To this purpose, the diamond punch geometry was calibrated from 1000 nm deep references measurements in fused silica and the machine frame stiffness value was refined so as to obtain a constant ratio between stiffness squared and load during indentation of the samples. The conversion of the reduced moduli to a uniaxial Young's moduli was performed assuming a Poisson's ratios of 0.24 and 0.29, respectively for  $\text{ReN}_2$  and  $\text{Re}$ <sup>51</sup>.

### *Temperature-dependent resistance measurements*

The resistance of the sample was measured by four-probe method passing a constant DC 90mA current through the sample and measuring both current and voltage drop across the sample. Temperature was measured using the S-type thermocouple.

### *Theoretical calculations*

The *ab initio* electronic structure calculations of  $\text{ReN}_2$  (12 atoms),  $\text{ReN}$  (2 atoms) and  $\text{ReN}_x$  ( $2 \times 3 \times 2$  supercell) were performed using the all electron projector-augmented-wave (PAW) method<sup>52</sup> as implemented in the VASP code<sup>53-55</sup>. Among the tested exchange-correlation potentials (PBE<sup>56</sup>, PBEsol<sup>57</sup>, AM05<sup>58</sup>) the PBEsol approximation has resulted into the best agreement between the derived experimental and theoretical equation of state. Convergence has been obtained with 700 eV energy cutoff for the plane wave basis and a ( $18 \times 10 \times 14$ ) Monkhorst-Pack k-points<sup>59</sup> type sampling of the Brillouin zone for  $\text{ReN}_2$ . Gaussian smearing technique was chosen with smearing of 0.05 eV. The convergence criterion for the electronic subsystem has been chosen to be equal to  $10^{-4}$  eV for two subsequent iterations, and the ionic relaxation loop within the conjugated gradient method was stopped

when forces became of the order of  $10^{-3}$  eV/Å. The elastic tensor  $C_{ij}$  has been calculated from the total energy applying (+/-) 1 and 2% lattice distortions. The Born mechanical stability conditions have been verified using the elastic constants. The phonon calculations have been performed within quasiharmonic approximation at temperature  $T = 0$  K using the finite displacement approach implemented into PHONOPY software<sup>60</sup>. Converged phonon dispersion relations have been achieved using a (3×3×3) supercell with 324 atoms and (5×5×5) Monkhorst-Pack  $k$ -point sampling.

### **Author contributions**

M.B., L.D., and ND designed the research, M.B., L.D., N.D., I.A.A. wrote the manuscript, M.B., L.D., S.C, T.F, G.A., V.B.P., E.G., M.H., A.P. H.-P.L. performed X-ray diffraction experiments, M.B. analyzed the X-ray diffraction data, F.T, A.V.P., I.A. performed theoretical calculations, H.F., M.B., T.K., S.V., W.S. performed synthesis in the large volume press and the synthesis of precursors. B.M. and P.F. performed nanoindentation measurements. L.D. performed electrical resistance measurements. All authors contributed to the discussion of the results.

### **Acknowledgements**

M.B. thanks the Deutsche Forschungsgemeinschaft (DFG project BY112/1-1). N.D. and L.D. thank the Deutsche Forschungsgemeinschaft (DFG projects DU 954-11/1 and DU 393-10/1) and the Federal Ministry of Education and Research, Germany (BMBF, grant no. 5K16WC1) for financial support. S.V. and W.S. are grateful for a PhD fellowship granted by the Fonds der Chemischen Industrie (FCI), Germany. B.M. thanks the Deutsche Forschungsgemeinschaft (DFG project ME 4368/7-1) for financial support. Parts of this research were carried out at the Extreme Conditions Beamline (P02.2) at DESY, a member of Helmholtz Association (HGF). Portions of this work was performed at GeoSoilEnviroCARS (The University of Chicago, Sector 13), Advanced Photon Source (APS), Argonne National Laboratory. GeoSoilEnviroCARS is supported by the National Science Foundation - Earth Sciences (EAR - 1634415) and Department of Energy- GeoSciences (DE-FG02-94ER14466). This research used resources of the Advanced Photon Source, a U.S. Department of Energy (DOE) Office of Science User Facility operated for the DOE Office of Science by Argonne National Laboratory under Contract No. DE-AC02-06CH11357, as well as resources from the Center for Nanoanalysis and Electron Microscopy (CENEM) at Friedrich-Alexander University Erlangen-Nürnberg. Several high-pressure diffraction experiments were performed on beamline ID15B

at the European Synchrotron Radiation Facility (ESRF), Grenoble, France. We thank Sven Linhardt and Gerald Bauer for the help with electrical resistance measurements.

## References

1. Bhadram, V. S. *et al.* Semiconducting cubic titanium nitride in the Th<sub>3</sub>P<sub>4</sub> structure. *Phys. Rev. Mater.* **2**, 011602 (2018).
2. Steele, B. A. *et al.* High-Pressure Synthesis of a Pentazolate Salt. *Chem. Mater.* **29**, 735–741 (2017).
3. Struzhkin, V. V. *et al.* Synthesis of sodium polyhydrides at high pressures. *Nat. Commun.* **7**, 12267 (2016).
4. Yeung, M. T., Mohammadi, R. & Kaner, R. B. Ultraincompressible, Superhard Materials. *Annu. Rev. Mater. Res.* **46**, 465–485 (2016).
5. Cumberland, R. W. *et al.* Osmium diboride, an ultra-incompressible, hard material. *J. Am. Chem. Soc.* **127**, 7264–7265 (2005).
6. Qin, J. *et al.* Is Rhenium Diboride a Superhard Material? *Adv. Mater.* **20**, 4780–4783 (2008).
7. Dubrovinskaia, N., Dubrovinsky, L. & Solozhenko, V. L. Comment on ‘synthesis of ultra-incompressible superhard rhenium diboride at ambient pressure’. *Science* **318**, 1550 (2007).
8. Chung, H.-Y. H.-Y. *et al.* Synthesis of Ultra-Incompressible Superhard Rhenium Diboride at Ambient Pressure. *Science* **316**, 436–439 (2007).
9. Gou, H. *et al.* Discovery of a Superhard Iron Tetraboride Superconductor. *Phys. Rev. Lett.* **111**, 157002 (2013).
10. Mohammadi, R. *et al.* Tungsten tetraboride, an inexpensive superhard material. *Proc. Natl. Acad. Sci. U. S. A.* **108**, 10958–10962 (2011).
11. Andersen, T., Haugen, H. K. & Hotop, H. Binding Energies in Atomic Negative Ions : III. *J. Phys. Chem. Ref. data* **28**, 1511–1533 (1999).
12. Richter, T. & Niewa, R. Chemistry of Ammonothermal Synthesis. *Inorganics* **2**, 29–78 (2014).
13. Häusler, J. & Schnick, W. Ammonothermal Synthesis of Nitrides: Recent Developments and Future Perspectives. *Chem. - Eur. J.* 1–17 (2018). doi:10.1002/chem.201800115
14. Sun, W. *et al.* Thermodynamic Routes to Novel Metastable Nitrogen-Rich Nitrides. *Chem. Mater.* **29**, 6936–6946 (2017).

15. Crowhurst, J. C. *et al.* Synthesis and Characterization of the Nitrides of Platinum and Iridium. *Science* **311**, 1275–1278 (2006).
16. Crowhurst, J. C. *et al.* Synthesis and characterization of nitrides of iridium and palladium. *J. Mater. Res.* **23**, 1–5 (2008).
17. Young, A. F. *et al.* Synthesis of Novel Transition Metal Nitrides IrN<sub>2</sub> and OsN<sub>2</sub>. *Phys. Rev. Lett.* **96**, 155501 (2006).
18. Bhadram, V. S., Kim, D. Y. & Strobel, T. A. High-Pressure Synthesis and Characterization of Incompressible Titanium Pernitride. *Chem. Mater.* **28**, 1616–1620 (2016).
19. Niwa, K. *et al.* High pressure synthesis of marcasite-type rhodium pernitride. *Inorg. Chem.* **53**, 697–699 (2014).
20. Niwa, K. *et al.* Discovery of the Last Remaining Binary Platinum-Group Pernitride RuN<sub>2</sub>. *Chem. - Eur. J.* **20**, 13885–13888 (2014).
21. Niwa, K. *et al.* Highly Coordinated Iron and Cobalt Nitrides Synthesized at High Pressures and High Temperatures. *Inorg. Chem.* **56**, 6410–6418 (2017).
22. Bykov, M. *et al.* Fe-N system at high pressure reveals a compound featuring polymeric nitrogen chains. *Nat. Commun.* **9**, 2756 (2018).
23. Friedrich, A. *et al.* Novel Rhenium Nitrides. *Phys. Rev. Lett.* **105**, 085504 (2010).
24. Zhao, Z. *et al.* Nitrogen concentration driving the hardness of rhenium nitrides. *Sci. Rep.* **4**, 4797 (2014).
25. Kawamura, F., Yusa, H. & Taniguchi, T. Synthesis of rhenium nitride crystals with MoS<sub>2</sub> structure. *Appl. Phys. Lett.* **100**, 2–5 (2012).
26. Wang, Y., Yao, T., Yao, J.-L., Zhang, J. & Gou, H. Does the real ReN<sub>2</sub> have the MoS<sub>2</sub> structure? *Phys. Chem. Chem. Phys.* **15**, 183–187 (2013).
27. Bykov, M. *et al.* High-Pressure Synthesis of a Nitrogen-Rich Inclusion Compound ReN<sub>8</sub>·xN<sub>2</sub> with Conjugated Polymeric Nitrogen Chains. *Angew. Chem., Int. Ed.* **57**, 9048–9053 (2018).
28. Klotz, S., Chervin, J.-C., Munsch, P., Le Marchand, G. & Marchand, G. Le. Hydrostatic limits of 11 pressure transmitting media. *J. Phys. D. Appl. Phys.* **42**, 075413 (2009).
29. Angel, R. J. Equations of state. *Rev. Mineral. Geochemistry* **41**, 35–60 (2000).
30. Chen, X.-J. *et al.* Hard superconducting nitrides. *Proc. Natl. Acad. Sci.* **102**, 3198–3201 (2005).
31. Wu, Z. *et al.* Crystal structures and elastic properties of superhard IrN<sub>2</sub> and IrN<sub>3</sub>. *Phys.*

- Rev. B* **76**, 054115 (2007).
32. Chen, Z. W. *et al.* Crystal structure and physical properties of OsN<sub>2</sub> and PtN<sub>2</sub> in the marcasite hase. *Phys. Rev. B* **75**, 054103 (2007).
  33. Nye, J. F. *Physical Properties of Crystals*. (Clarendon Press, 1985).
  34. Wessel, M. & Dronskowski, R. Nature of N-N bonding within high-pressure noble-metal pernitrides and the prediction of lanthanum pernitride. *J. Am. Chem. Soc.* **132**, 2421–2429 (2010).
  35. Hill, R. The Elastic Behaviour of a Crystalline Aggregate. *Proc. Phys. Soc. Sect. A* **65**, 349–354 (1952).
  36. Yu, S., Zeng, Q., Oganov, A. R., Frapper, G. & Zhang, L. Phase stability , chemical bonding and mechanical study. *Phys. Chem. Chem. Phys.* **17**, 11763–11769 (2015).
  37. Jhi, S., Ihm, J., Louie, S. G. & Cohen, M. L. Electronic mechanism of hardness enhancement in transition-metal carbonitrides. *Nature* **399**, 132–134 (1999).
  38. Dubrovinsky, L., Dubrovinskaia, N., Prakapenka, V. B. & Abakumov, A. M. Implementation of micro-ball nanodiamond anvils for high-pressure studies above 6 Mbar. *Nat. Commun.* **3**, 1163 (2012).
  39. Zha, C.-S., Bassett, W. A. & Shim, S.-H. Rhenium, an in situ pressure calibrant for internally heated diamond anvil cells. *Rev. Sci. Instrum.* **75**, 2409–2418 (2004).
  40. Anzellini, S., Dewaele, A., Occelli, F., Loubeyre, P. & Mezouar, M. Equation of state of rhenium and application for ultra high pressure calibration. *J. Appl. Phys.* **115**, 043511 (2014).
  41. Ishii, T. *et al.* Generation of pressures over 40 GPa using Kawai-type multi-anvil press with tungsten carbide anvils. *Rev. Sci. Instrum.* **87**, (2016).
  42. Frierson, W. J. & Filbert, W. F. Ammonium Azide. *Inorganic Syntheses* (1946).  
doi:10.1002/9780470132333.ch39
  43. Fei, Y. *et al.* Toward an internally consistent pressure scale. *Proc. Natl. Acad. Sci.* **104**, 9182–9186 (2007).
  44. Liermann, H.-P. *et al.* The Extreme Conditions Beamline P02.2 and the Extreme Conditions Science Infrastructure at PETRA III. *J. Synchrotron Radiat.* **22**, 908–924 (2015).
  45. Prescher, C. & Prakapenka, V. B. DIOPTAS: A program for reduction of two-dimensional X-ray diffraction data and data exploration. *High Press. Res.* **35**, 223–230 (2015).
  46. Sheldrick, G. M. SHELXT – Integrated space-group and crystal-structure



- determination. *Acta Crystallogr. Sect. A Found. Adv.* **71**, 3–8 (2015).
47. Petříček, V., Dušek, M. & Plášil, J. Crystallographic computing system Jana2006: solution and refinement of twinned structures. *Zeitschrift für Krist. - Cryst. Mater.* **231**, 583–599 (2016).
  48. Merle, B., Maier-Kiener, V. & Pharr, G. M. Influence of modulus-to-hardness ratio and harmonic parameters on continuous stiffness measurement during nanoindentation. *Acta Mater.* **134**, 167–176 (2017).
  49. Oliver, W. C. & Pharr, G. M. An improved technique for determining hardness and elastic modulus using load and displacement sensing indentation experiments. *J. Mater. Res.* **7**, 1564–1583 (1992).
  50. Oliver, W. C. & Pharr, G. M. Measurement of hardness and elastic modulus by instrumented indentation: Advances in understanding and refinements to methodology. *J. Mater. Res.* **19**, 3–20 (2004).
  51. Simmons, G. & Wang, H. *Single Crystal Elastic Constants and Calculated Aggregate Properties. A Handbook.* (The MIT Press, 1971).
  52. Blöchl, P. E. Projector augmented-wave method. *Phys. Rev. B* **50**, 17953–17979 (1994).
  53. Kresse, G. & Furthmüller, J. Efficient iterative schemes for ab initio total-energy calculations using a plane-wave basis set. *Phys. Rev. B* **54**, 11169–11186 (1996).
  54. Kresse, G. & Furthmüller, J. Efficiency of ab-initio total energy calculations for metals and semiconductors using a plane-wave basis set. *Comput. Mater. Sci.* **6**, 15–50 (1996).
  55. Kresse, G. & Joubert, D. From ultrasoft pseudopotentials to the projector augmented-wave method. *Phys. Rev. B* **59**, 1758–1775 (1999).
  56. Perdew, J. P., Burke, K. & Ernzerhof, M. Generalized Gradient Approximation Made Simple. *Phys. Rev. Lett.* **77**, 3865–3868 (1996).
  57. Csonka, I. *et al.* Restoring the Density-Gradient Expansion for Exchange in Solids and Surfaces. *Phys. Rev. Lett.* **100**, 136406 (2008).
  58. Armiento, R. & Mattsson, A. E. Functional designed to include surface effects in self-consistent density functional theory. *Phys. Rev. B* **72**, 085108 (2005).
  59. Monkhorst, H. J. & Pack, J. D. Special points for Brillouin-zone integrations. *Phys. Rev. B* **13**, 5188–5192 (1976).
  60. Togo, A. & Tanaka, I. First principles phonon calculations in materials science. *Scr. Mater.* **108**, 1–5 (2015).
  38. Dubrovinsky, L., Dubrovinskaia, N., Prakapenka, V. B. & Abakumov, A. M.

- Implementation of micro-ball nanodiamond anvils for high-pressure studies above 6 Mbar. *Nat. Commun.* **3**, 1163 (2012).
39. Zha, C.-S., Bassett, W. A. & Shim, S.-H. Rhenium, an in situ pressure calibrant for internally heated diamond anvil cells. *Rev. Sci. Instrum.* **75**, 2409–2418 (2004).
  40. Anzellini, S., Dewaele, A., Occelli, F., Loubeyre, P. & Mezouar, M. Equation of state of rhenium and application for ultra high pressure calibration. *J. Appl. Phys.* **115**, 043511 (2014).
  41. Ishii, T. *et al.* Generation of pressures over 40 GPa using Kawai-type multi-anvil press with tungsten carbide anvils. *Rev. Sci. Instrum.* **87**, (2016).
  42. Frierson, W. J. & Filbert, W. F. Ammonium Azide. *Inorganic Syntheses* (1946). doi:10.1002/9780470132333.ch39
  43. Fei, Y. *et al.* Toward an internally consistent pressure scale. *Proc. Natl. Acad. Sci.* **104**, 9182–9186 (2007).
  44. Liermann, H.-P. *et al.* The Extreme Conditions Beamline P02.2 and the Extreme Conditions Science Infrastructure at PETRA III. *J. Synchrotron Radiat.* **22**, 908–924 (2015).
  45. Prescher, C. & Prakapenka, V. B. DIOPTAS: A program for reduction of two-dimensional X-ray diffraction data and data exploration. *High Press. Res.* **35**, 223–230 (2015).
  46. Sheldrick, G. M. SHELXT – Integrated space-group and crystal-structure determination. *Acta Crystallogr. Sect. A Found. Adv.* **71**, 3–8 (2015).
  47. Petříček, V., Dušek, M. & Plášil, J. Crystallographic computing system Jana2006: solution and refinement of twinned structures. *Zeitschrift für Krist. - Cryst. Mater.* **231**, 583–599 (2016).
  48. Merle, B., Maier-Kiener, V. & Pharr, G. M. Influence of modulus-to-hardness ratio and harmonic parameters on continuous stiffness measurement during nanoindentation. *Acta Mater.* **134**, 167–176 (2017).
  49. Oliver, W. C. & Pharr, G. M. An improved technique for determining hardness and elastic modulus using load and displacement sensing indentation experiments. *J. Mater. Res.* **7**, 1564–1583 (1992).
  50. Oliver, W. C. & Pharr, G. M. Measurement of hardness and elastic modulus by instrumented indentation: Advances in understanding and refinements to methodology. *J. Mater. Res.* **19**, 3–20 (2004).
  51. Simmons, G. & Wang, H. *Single Crystal Elastic Constants and Calculated Aggregate*

- Properties. A Handbook.* (The MIT Press, 1971).
52. Blöchl, P. E. Projector augmented-wave method. *Phys. Rev. B* **50**, 17953–17979 (1994).
  53. Kresse, G. & Furthmüller, J. Efficient iterative schemes for ab initio total-energy calculations using a plane-wave basis set. *Phys. Rev. B* **54**, 11169–11186 (1996).
  54. Kresse, G. & Furthmüller, J. Efficiency of ab-initio total energy calculations for metals and semiconductors using a plane-wave basis set. *Comput. Mater. Sci.* **6**, 15–50 (1996).
  55. Kresse, G. & Joubert, D. From ultrasoft pseudopotentials to the projector augmented-wave method. *Phys. Rev. B* **59**, 1758–1775 (1999).
  56. Perdew, J. P., Burke, K. & Ernzerhof, M. Generalized Gradient Approximation Made Simple. *Phys. Rev. Lett.* **77**, 3865–3868 (1996).
  57. Csonka, I. *et al.* Restoring the Density-Gradient Expansion for Exchange in Solids and Surfaces. *Phys. Rev. Lett.* **100**, 136406 (2008).
  58. Armiento, R. & Mattsson, A. E. Functional designed to include surface effects in self-consistent density functional theory. *Phys. Rev. B* **72**, 085108 (2005).
  59. Monkhorst, H. J. & Pack, J. D. Special points for Brillouin-zone integrations. *Phys. Rev. B* **13**, 5188–5192 (1976).
  60. Togo, A. & Tanaka, I. First principles phonon calculations in materials science. *Scr. Mater.* **108**, 1–5 (2015).

## Supplementary Information

### **High-pressure synthesis of ultraincompressible hard rhenium nitride pernitride $\text{Re}_2(\text{N}_2)\text{N}_2$ stable at ambient conditions**

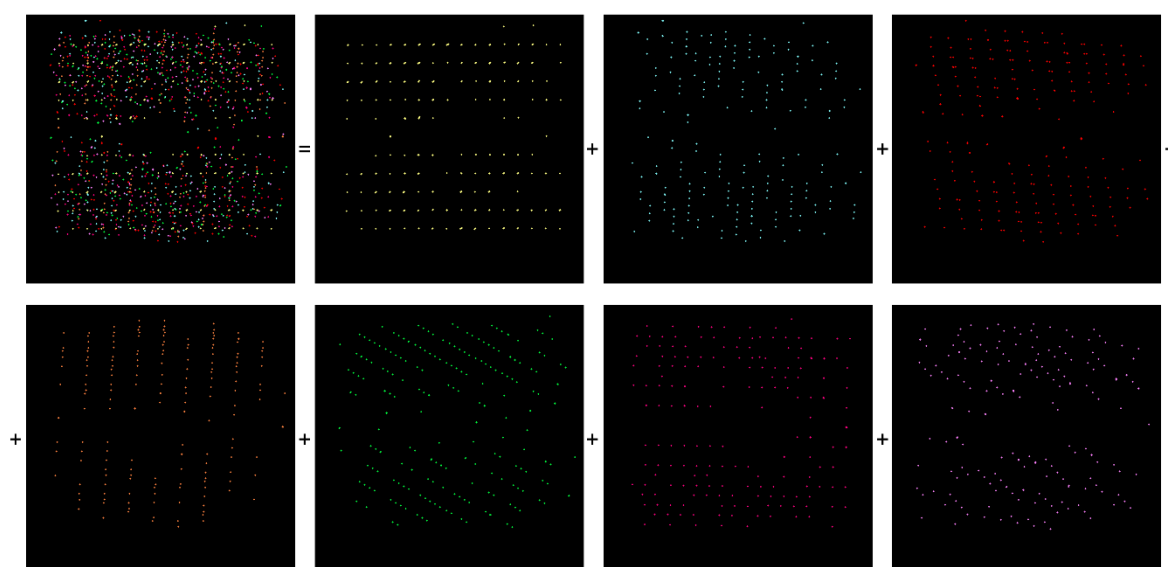
Maxim Bykov, Stella Chariton, Hongzhan Fei, Timofey Fedotenko, Georgios Aprilis, Alena V. Ponomareva, Ferenc Tasnádi, Igor A. Abrikosov, Benoit Merle, Patrick Feldner, Sebastian Vogel, Wolfgang Schnick, Eran Greenberg, Vitali Prakapenka, Michael Hanfland, Anna Pakhomova, Hanns-Peter Liermann, Tomoo Katsura, Natalia Dubrovinskaia, Leonid Dubrovinsky

### **Contents**

Analysis of multigrain/multiphase datasets.....	21
Estimation of the nitrogen content in the WC-type $\text{ReN}_x$ .....	22
Refinement and crystal structure details of $\text{ReN}_2$ .....	24
Compressibility of $\text{ReN}_2$ .....	25
Representative powder diffraction patterns. Synthesis of $\text{ReN}_2$ <i>via</i> a reaction with nitrogen .	25
Choice of solid nitrogen precursors .....	27
Synthesis of $\text{ReN}_2$ in a multianvil apparatus .....	29
Supplementary references .....	31

## Analysis of multigrain/multiphase datasets

If a chemical reaction occurs in a DAC during laser heating, it often leads to multiple domains of well-crystallized phase(s). Moreover, the diffraction spots originating from different grains not often overlap with each other and this allows to integrate the dataset separately for each grain. The same happened in a case of the Re – N<sub>2</sub> system. For the unit cell determination, we use the reciprocal space viewer (Ewald explorer) from *CrysAlis<sup>Pro</sup>*. It allows to manually select the reciprocal lattice of the grain. Below we provide an example for the typical dataset of ReN<sub>2</sub>. The Supplementary Figure 1 demonstrates the reciprocal space reconstruction with seven strongest lattices corresponding to the grains of ReN<sub>2</sub> in different orientations. The Supplementary Table 1 shows typical statistics for total/overlapped reflections in our datasets.



**Supplementary Figure 1.** Reciprocal space reconstruction with seven strongest lattices.

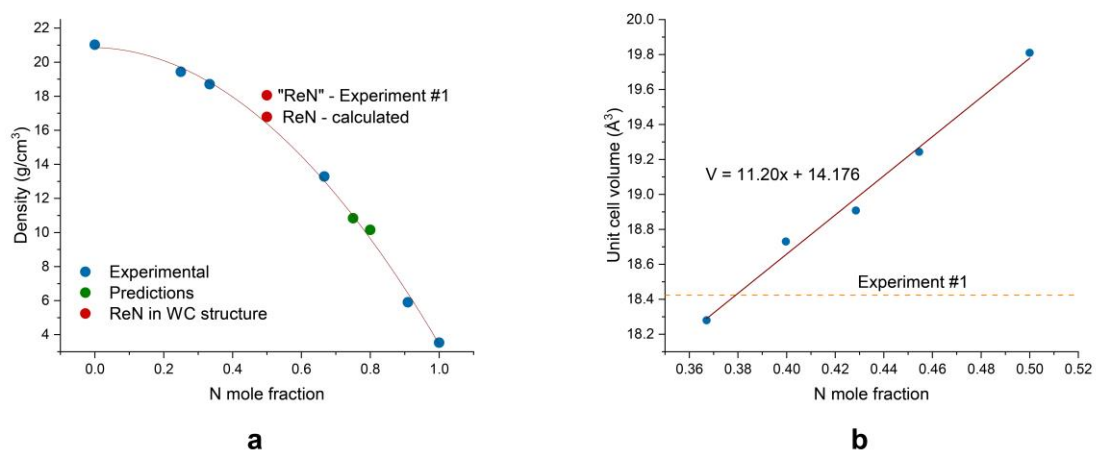
**Supplementary Table 1.** Typical reflection statistics for several ReN<sub>2</sub> grains, producing the strongest diffraction spots.

Grain	$a$ , Å	$b$ , Å	$c$ , Å	$\beta$ , °	$V$ , Å <sup>3</sup>	Reflections		
						total	separate	overlapped
#1	3.5065	6.1482	4.6884	111.175	94.3	249	249	0
#2	3.5065	6.1544	4.6865	111.253	94.3	218	216	2
#3	3.5072	6.1467	4.6921	111.197	94.3	249	246	3
#4	3.5022	6.1615	4.6885	111.099	94.4	196	194	2
#5	3.5020	6.1620	4.6906	111.214	94.4	243	237	6
#6	3.5031	6.1528	4.6933	111.212	94.3	198	190	8
#7	3.4967	6.1539	4.6939	111.149	94.2	208	199	9

## Estimation of the nitrogen content in the WC-type $\text{ReN}_x$

The ambient-pressure unit cell parameters and the unit cell volume of the WC-type  $\text{ReN}_x$  phase, obtained in the experiments #1 and #7 do not agree with our and with previous theoretical calculations if  $x = 1$  (Supplementary Table 2). Furthermore, the density of WC- $\text{ReN}$  phase with ideal 1:1 stoichiometry from theoretical calculations is in a good agreement with the N-content – density trend of the Re-N system (Supplementary Figure 2a). However, the experimental density, calculated with the assumption of 1:1 composition, is clearly higher than expected (Supplementary Figure 2a). In order to estimate the nitrogen content, we have calculated the unit cell volumes of  $\text{ReN}_x$  with  $x$  varying from 0.58 to 1 (Supplementary Table 2, Supplementary Figure 2b). In the studied composition range, the dependence of the unit cell volume of  $\text{ReN}_x$  linearly depends on the nitrogen content. The result of the linear fit, presented in the Supplementary Figure 2b was used to estimate the composition of  $\text{ReN}_x$  obtained in the experiments #1 and #6.

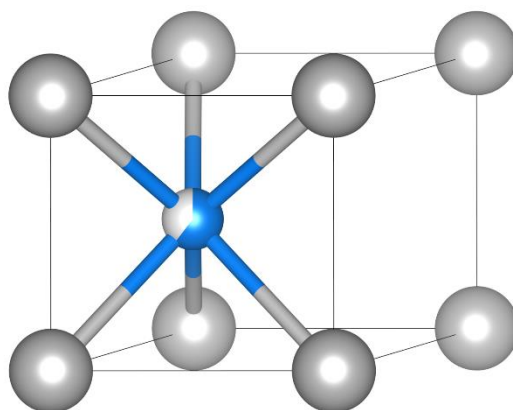
We could not reliably detect  $\text{ReN}_{0.6}$  phase in the experiment #2, which was used for the measurement of the equation of state. We would like to note here that the volume change of  $\text{ReN}_{0.6}$  between 0 and 42 GPa from the available single-crystal data is only -9.75%, which makes it a very incompressible compound as well. Several theoretical works were devoted to the  $\text{ReN}$  compound and it was predicted that the most stable structure of  $\text{ReN}$  is NiAs like structure.<sup>1,2</sup> We believe that the role of vacancies in the stabilization of  $\text{ReN}_x$  ( $x \leq 1$ ) phases must be taken into account in further theoretical calculations.



**Supplementary Figure 2.** (a) Density of Re-N compounds as a function of nitrogen content at ambient pressure. Blue points – experimental data on  $\text{Re}$ ,<sup>3</sup>  $\text{Re}_3\text{N}$ ,<sup>4</sup>  $\text{Re}_2\text{N}$ ,<sup>4</sup>  $\text{ReN}_2$  (this study),  $\text{ReN}_{10}$ ,<sup>5</sup> *cg-N*.<sup>6</sup> Green points – theoretically predicted compounds  $\text{ReN}_3$  and  $\text{ReN}_4$ .<sup>7</sup> Red points – calculated and experimental density of  $\text{ReN}$  in WC structure type. (b) Unit cell volume of WC-type Re-N phase as a function of nitrogen concentration. Blue points – calculated volumes of  $\text{ReN}_{0.58}$ ,  $\text{ReN}_{0.666}$ ,  $\text{ReN}_{0.75}$ ,  $\text{ReN}_{5/6}$  and  $\text{ReN}$ . Red line – linear fit.

**Supplementary Table 2.** Calculated and experimental lattice parameters for WC-type structure of  $\text{ReN}_x$  at ambient pressure.

	$V, \text{\AA}^3$	Method	Reference
<b>Experiments:</b>			
Experiment #1	18.424	SC XRD	This study
Experiment #6	18.19	SC XRD	This study
<b>Calculations:</b>			
ReN	19.46	LDA	1
		TB-LMTO	
ReN	19.64	GGA-PBE	8
ReN	19.31	LDA, FP-LAPW	2
ReN	19.81	PBEsol	This study
$\text{ReN}_{5/6}$	19.24	PBEsol	This study
$\text{ReN}_{0.75}$	18.91	PBEsol	This study
$\text{ReN}_{0.666}$	18.73	PBEsol	This study
$\text{ReN}_{0.58}$	18.28	PBEsol	This study



**Supplementary Figure 3.** The crystal structure of  $\text{ReN}_{0.6}$  at ambient conditions. Re atoms – gray balls, N atoms – blue.

## Refinement and crystal structure details of ReN<sub>2</sub>

**Supplementary Table 3.** Details on the refinement of the crystal structure of ReN<sub>2</sub> at ambient conditions

<b>Crystal data</b>	
Chemical formula	ReN <sub>2</sub>
$M_r$ , g/mol	214.22
Crystal system, space group	Monoclinic, $P2_1/c$ (No. 14)
Temperature (K)	293
Pressure (GPa)	0.0001
$a, b, c$ (Å)	3.6254(17), 6.407(7), 4.948(3)
$\beta$ (°)	111.48(6)
$V$ (Å <sup>3</sup> )	106.96(15)
$Z$	4
Radiation type	Synchrotron, $\lambda = 0.2903$ Å
$\mu$ (mm <sup>-1</sup> )	10.76
Crystal size (mm <sup>3</sup> )	0.03 × 0.02 × 0.01
<b>Data collection</b>	
Diffractometer	13IDD, APS, Chicago, USA
Absorption correction	Multi-scan
$T_{\min}, T_{\max}$	0.386, 1.000
No. of measured, independent and observed [ $I > 2\sigma(I)$ ] reflections	290, 180, 175
$R_{\text{int}}$	0.011
$(\sin \theta/\lambda)_{\text{max}}$ (Å <sup>-1</sup> )	0.879
<b>Refinement</b>	
$R[F^2 > 2\sigma(F^2)], wR(F^2), S$	0.035, 0.088, 1.10
No. of reflections	180
No. of parameters	19
$\Delta\rho_{\text{max}}, \Delta\rho_{\text{min}}$ (e Å <sup>-3</sup> )	2.83, -2.67
<b>Refined crystal structure</b>	
Re ( $x, y, z$ )	0.35490(11), 0.34041(8), 0.19965(8)
N1 ( $x, y, z$ )	0.194(2), 0.038(2), 0.311(19)
N2 ( $x, y, z$ )	0.259(3), 0.6381(18), 0.024(2)
<b>Calculated crystal structure</b>	
Re ( $x, y, z$ )	(0.35397, 0.33961, 0.19931)
N1 ( $x, y, z$ )	(0.1889, 0.037, 0.30)
N2 ( $x, y, z$ )	(0.2540, 0.6397, 0.0164)



**Supplementary Table 4.** Selected geometric parameters of ReN<sub>2</sub> at ambient conditions (Å)

Re01—Re01 <sup>i</sup>	2.7318 (16)	Re01—N2 <sup>vi</sup>	2.095 (10)
Re01—Re01 <sup>ii</sup>	2.7318 (16)	N1—Re01 <sup>iv</sup>	2.112 (11)
Re01—N1	2.105 (12)	N1—Re01 <sup>ii</sup>	2.082 (9)
Re01—N1 <sup>iii</sup>	2.112 (11)	N1—N1 <sup>vii</sup>	1.412 (16)
Re01—N1 <sup>i</sup>	2.082 (9)	N2—Re01 <sup>v</sup>	2.082 (10)
Re01—N2	2.072 (11)	N2—Re01 <sup>vi</sup>	2.095 (9)
Re01—N2 <sup>iv</sup>	2.028 (11)	N2—Re01 <sup>iii</sup>	2.028 (11)
Re01—N2 <sup>v</sup>	2.082 (10)		

Symmetry code(s): (i)  $x, -y+1/2, z+1/2$ ; (ii)  $x, -y+1/2, z-1/2$ ; (iii)  $-x+1, y+1/2, -z+1/2$ ;

(iv)  $-x+1, y-1/2, -z+1/2$ ; (v)  $-x+1, -y+1, -z$ ; (vi)  $-x, -y+1, -z$ ; (vii)  $-x, -y, -z$ .

## Compressibility of ReN<sub>2</sub>

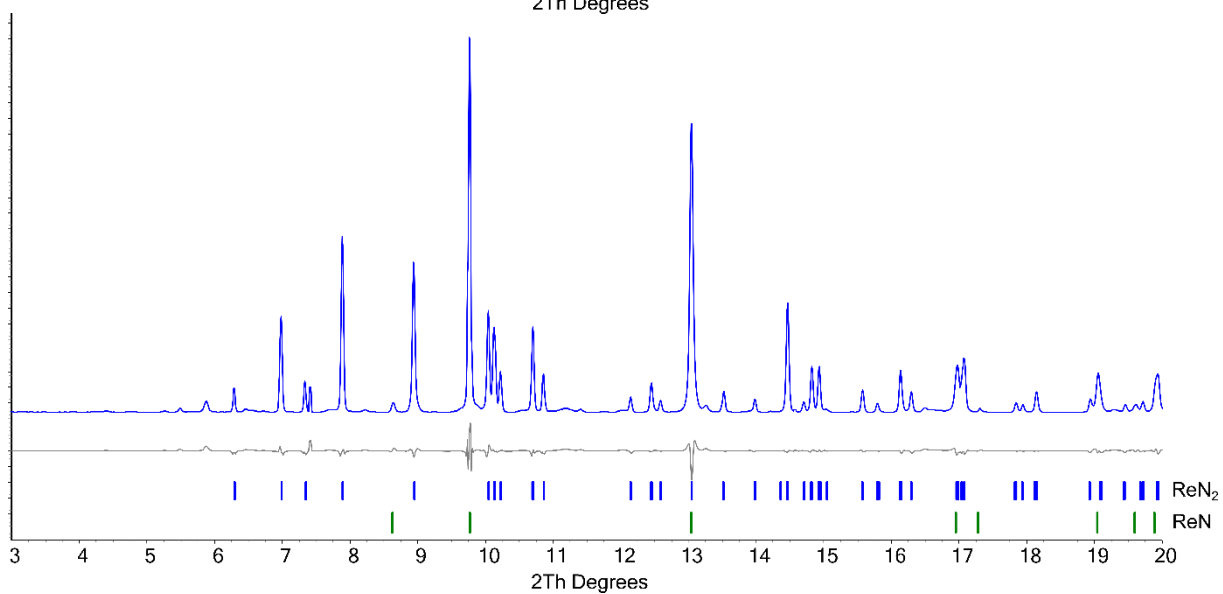
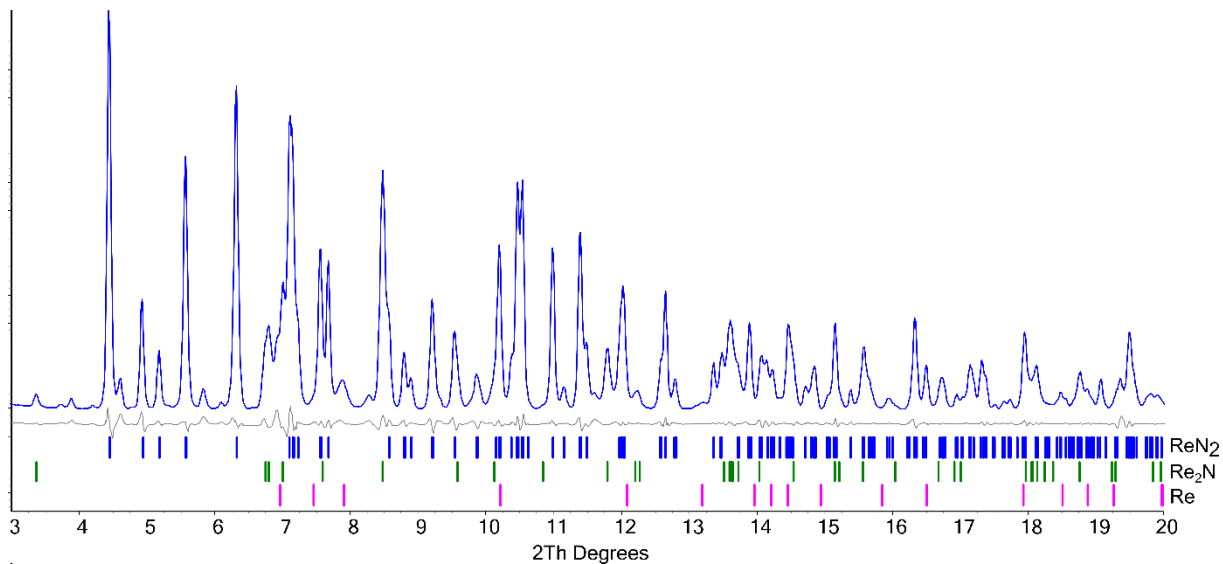
**Supplementary Table 5.** Experimental lattice parameters of ReN<sub>2</sub> on compression.

Pressure, GPa	$a, \text{Å}$	$b, \text{Å}$	$c, \text{Å}$	$\beta, ^\circ$	$V, \text{Å}^3$
0.0001	3.62565(16)	6.4216(2)	4.9478(3)	111.446(4)	107.218(9)
3.37(5)	3.6171(2)	6.4118(4)	4.9234(3)	111.250(5)	106.420(12)
4.10(5)	3.6154(3)	6.4106(6)	4.9161(6)	111.279(8)	106.173(19)
6.95(9)	3.6092(4)	6.3961(7)	4.9050(6)	111.256(8)	105.53(2)
8.97(6)	3.6055(3)	6.3872(8)	4.8974(6)	111.267(8)	105.10(2)
11.18(5)	3.5993(4)	6.3770(8)	4.8822(6)	111.261(11)	104.43(2)
12.79(11)	3.5957(4)	6.3723(8)	4.8715(9)	111.242(12)	104.03(3)
14.74(11)	3.5900(4)	6.3623(8)	4.8617(8)	111.177(12)	103.54(3)
17.97(13)	3.5849(5)	6.3517(8)	4.8523(6)	111.202(11)	103.01(2)
25.67(15)	3.5728(6)	6.3071(10)	4.8226(8)	111.243(14)	101.29(3)
32.11(17)	3.5604(6)	6.2742(10)	4.7992(8)	111.264(14)	99.91(3)
39.37(13)	3.5482(9)	6.2338(13)	4.7735(9)	111.272(17)	98.39(4)
45.44(14)	3.5379(9)	6.1963(10)	4.7503(8)	111.368(15)	96.98(4)

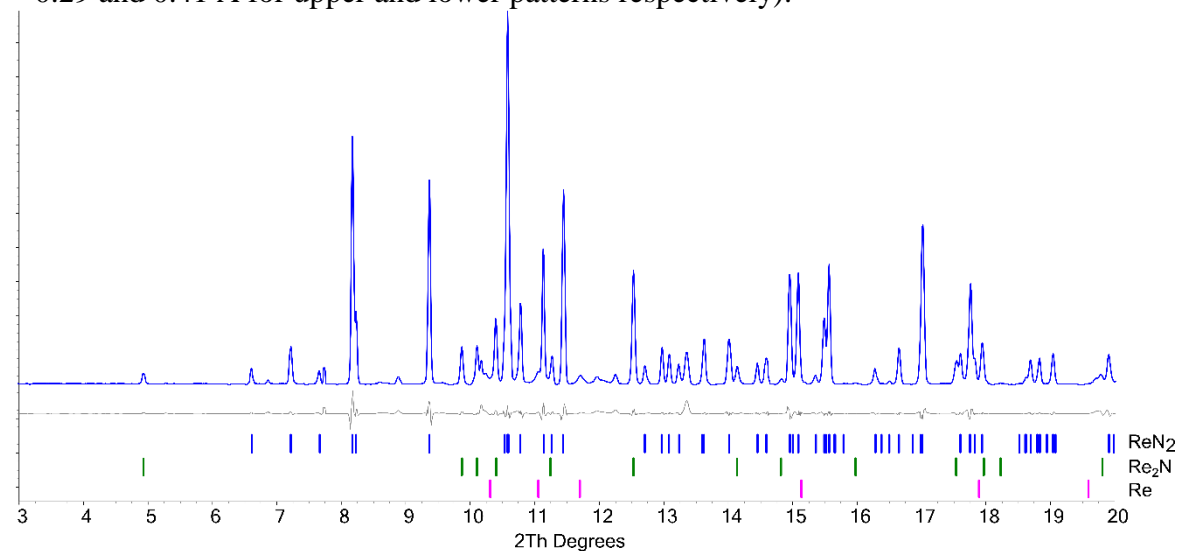
## Representative powder diffraction patterns. Synthesis of ReN<sub>2</sub> via a reaction with nitrogen

*Note 1:* Due to the small lattice parameters of defect WC-type ReN<sub>x</sub>, we could not reliably detect it on some powder patterns, where it could be in a mixture with ReN<sub>2</sub> and Re<sub>2</sub>N. Single-crystalline grains of ReN<sub>x</sub> were found only in the experiments #1 and #6, but we cannot exclude that this phase may be present in other syntheses.

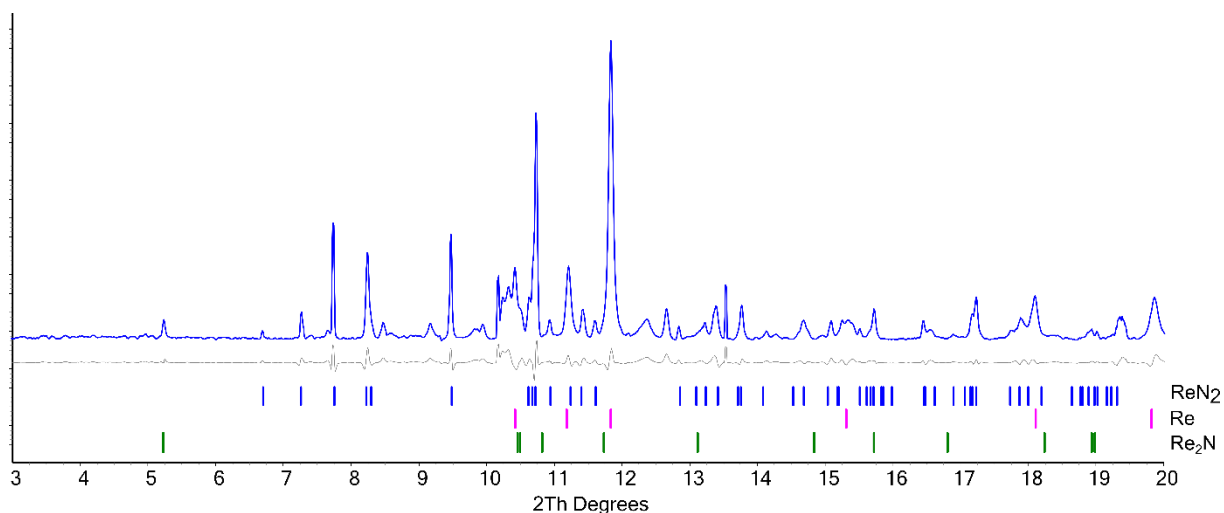
*Note 2:* Some powder diffraction patterns contain very weak non-indexed peaks. These peaks may originate from the pressure-transmitting medium (N<sub>2</sub>) or other minor phases. Le Bail fits were performed on the major phases, which have also been confirmed by the single-crystal experiments. Peak indexing of weak unknown phases based on the powder pattern in such a mixture would be unreliable.



**Supplementary Figure 4.** Powder diffraction pattern of the sample #1 at ambient pressure ( $\lambda = 0.29$  and  $0.41 \text{ \AA}$  for upper and lower patterns respectively).



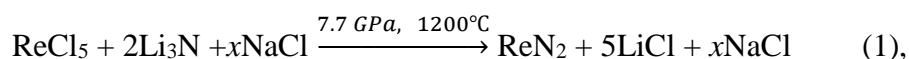
**Supplementary Figure 5.** Powder diffraction pattern of the sample #3 at 71 GPa ( $\lambda = 0.41 \text{ \AA}$ ).



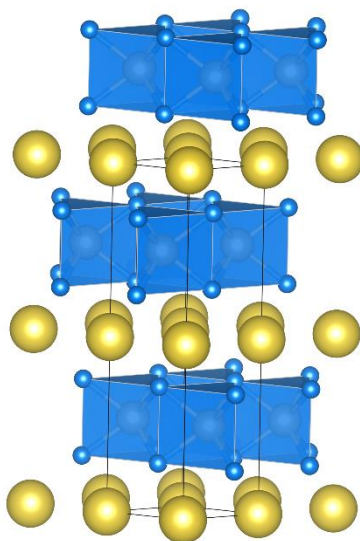
**Supplementary Figure 6.** Powder diffraction pattern of the sample #4 at 86 GPa ( $\lambda = 0.41 \text{ \AA}$ ).

### Choice of solid nitrogen precursors

The reaction between Re and  $\text{NaN}_3$  resulted in the main product, which has hexagonal symmetry  $P6_3/mmc$  ( $a = 2.7715$ ,  $c = 11.2191 \text{ \AA}$ ). The structure solution and refinement revealed its chemical formula as  $\text{NaReN}_2$ . The structure is based on layered  $\text{MoS}_2$ -type structure with sodium atoms intercalated between  $\text{ReN}_2$  layers (Supplementary Figure 7). Na occupies the crystallographic site  $2a$  ( $0, 0, 0$ ),  $\text{Re} - 2c$  ( $1/3, 2/3, 1/4$ ),  $\text{N} - 4f$  ( $1/3, 2/3, 0.6405$ ). It should be noted that the lattice parameters of this phase are very close to those of the  $\text{ReN}_2$  phase, that was synthesized by Kawamura *et al.*,<sup>9</sup> with a difference that the lattice parameter  $c$  of  $\text{NaReN}_2$  is larger. If we consider the reaction, reported by Kawamura *et al.*:<sup>9</sup>



we can notice two important problems: The equation is not balanced (and cannot be balanced, even if we consider the release of free nitrogen on the right side of the equation) and rhenium is the only element that has changed its oxidation state. We suggest that the real product of the reaction (1) is  $\text{LiReN}_2$ . This explains both issues mentioned above, and is in agreement with shorter  $c$ -axis than in  $\text{NaReN}_2$  due to the smaller cation radius of lithium compared to sodium.

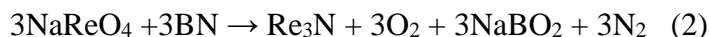


**Supplementary Figure 7.** The crystal structure of NaReN<sub>2</sub> from the synthesis #5 at ~40 GPa. Yellow balls – Na atoms. Blue polyhedra – ReN<sub>6</sub> trigonal prisms. Re occupies the site 2c (1/3, 2/3, 1/4), N – 4f (1/3, 2/3, 0.64217), Na – 2a (0 0 0).

Sodium azide appeared to be not a suitable source of nitrogen for high-pressure nitridation reaction, but opens a route to ternary nitrides with intercalated alkali metals, which in turn may be important for the development of high-performance electrode materials.<sup>10</sup>

The experiment in LHDAC with NH<sub>4</sub>N<sub>3</sub> as a source of nitrogen (Experiment #6, Table 1) resulted in the synthesis of ReN<sub>2</sub> and defect WC-type ReN<sub>x</sub>. The unit cell volume of WC-type ReN<sub>x</sub> at ambient pressure appeared to be slightly smaller than that in the Experiment#1 [ $V_{\text{exp1}} = 18.42(1) \text{ \AA}^3$ ,  $V_{\text{exp6}} = 18.19(1) \text{ \AA}^3$ ] and the estimated composition of this compound is ReN<sub>0.56</sub>. The Experiments #6 and 7 show that NH<sub>4</sub>N<sub>3</sub> precursor may be successfully used for the synthesis of rhenium nitrides when a solid source of nitrogen is required.

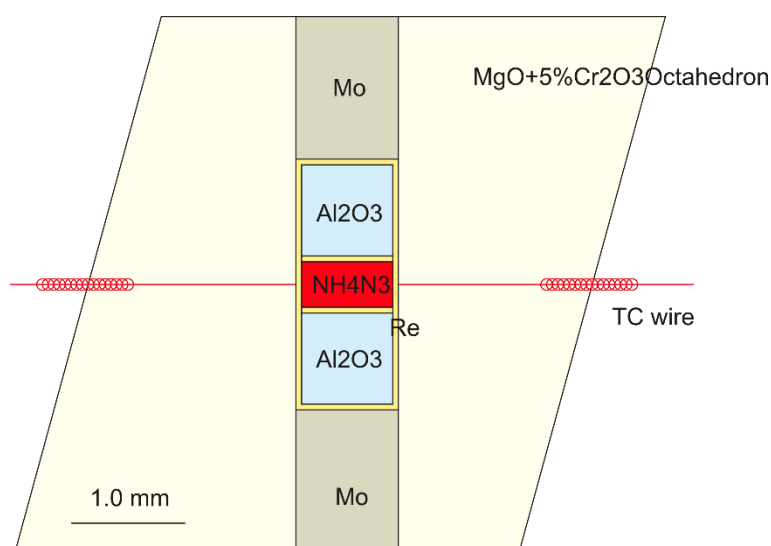
Currently, several methods are used for the synthesis of nitrides in the LVP. One route is a high-pressure solid-state metathesis (HPSSM) reaction between an oxidized metal precursor and a nitride (*e.g.* boron nitride BN or lithium nitride Li<sub>3</sub>N).<sup>9,11–14</sup> Recently Lei *et al.* reported a novel synthetic route to rhenium nitride Re<sub>3</sub>N:<sup>13,15</sup>



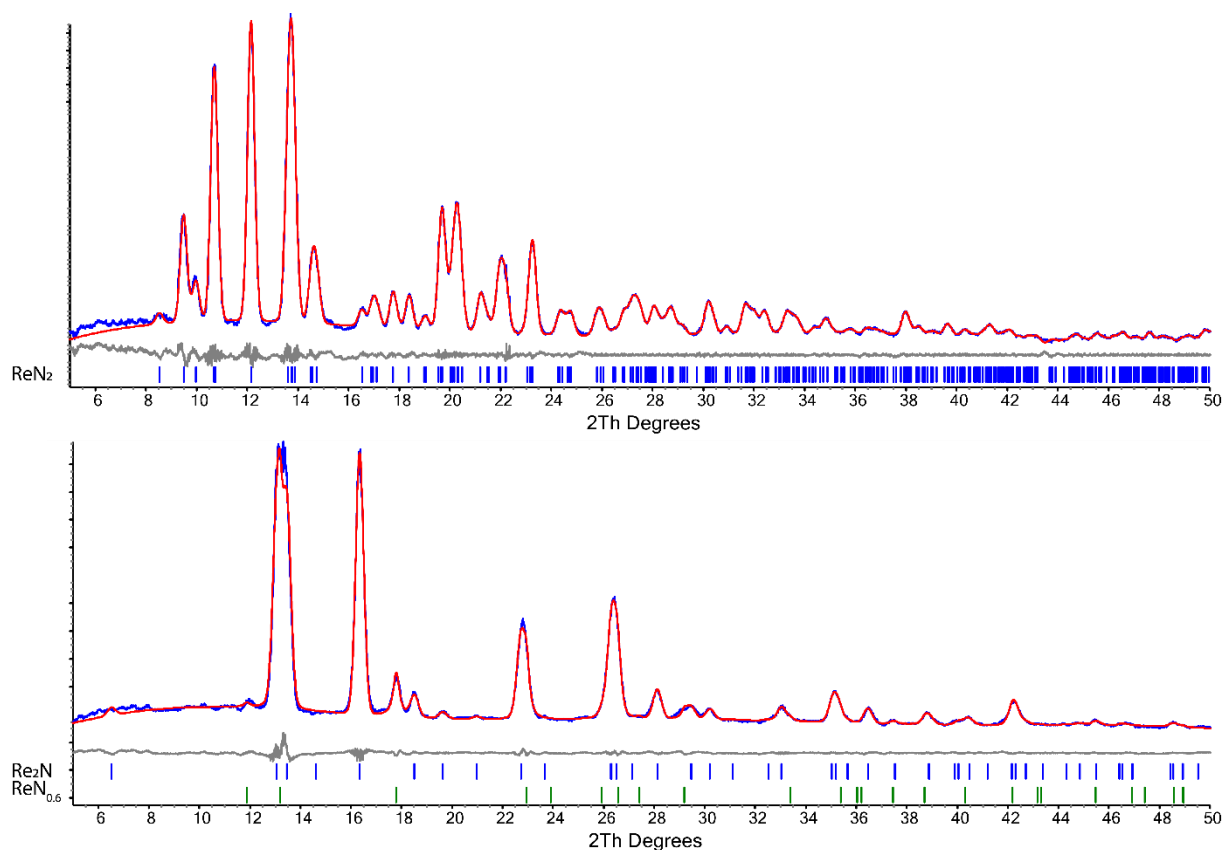
Although, the HPSSM method resulted in a number of exciting discoveries, it has a few disadvantages. In case of a simple metathesis reaction, where the oxidation state of elements is not changed it will not be possible to obtain compounds with N-N units. In case of redox reactions, where metal itself serves as an oxidizer of nitrogen, it is hard to create an excess of nitrogen that can prevent decomposition of target nitrogen-rich phases. Furthermore, there are

always several side products of such a reaction: *e.g.* the release of free oxygen like in the reaction (3) may influence the reaction in some cases. Schnick *et al.* successfully used controlled decomposition of azides to obtain diazenides  $\text{BaN}_2$ ,  $\text{SrN}_2$  and  $\text{CaN}_2$  as well as  $\text{Li}_2\text{N}_2$  in a large volume press.<sup>16,17</sup> This is a much cleaner method than a metathesis reaction, but is demanding, because not all metal azides are readily available and safe to work with.  $\text{NH}_4\text{N}_3$  appears to be a good choice for the synthesis of binary nitrides of transition metals due to several reasons: It has a high content of nitrogen (93.3 wt. %), and it can serve as an oxidizer, so that the elemental metal can be used for the reaction. Compared with the metal azides, it is relatively safe to work with this material. The dissociation of the excess of  $\text{NH}_4\text{N}_3$  may create high partial pressure of  $\text{N}_2$ , which prevents the decomposition of target nitrogen-rich phases (Le Chatelier principle).<sup>18</sup>

### Synthesis of $\text{ReN}_2$ in a multianvil apparatus



**Supplementary Figure 8.** Schematic drawing of high-pressure cell assembly for the multianvil synthesis of rhenium nitrides.



**Supplementary Figure 9.** Powder diffraction pattern of the samples recovered from the synthesis in the multianvil press (Experiment #7),  $\lambda = 0.56 \text{ \AA}$  (Ag-K $\alpha$ ).  $\text{ReN}_2$  and  $\text{Re}_2\text{N}$  phases were characterized by single-crystal X-ray diffraction, while  $\text{ReN}_{0.6}$  is evidenced only from the powder XRD.

## Supplementary references

1. Asvini meenaatci, A. T., Rajeswarapalanichamy, R. & Iyakutti, K. First-principles study of electronic structure of transition metal nitride: ReN under normal and high pressure. *Phys. B Condens. Matter* **406**, 3303–3307 (2011).
2. Li, Y.-L. & Zeng, Z. Potential ultra-incompressible material ReN: First-principles prediction. *Solid State Commun.* **149**, 1591–1595 (2009).
3. Dubrovinsky, L., Dubrovinskaia, N., Prakapenka, V. B. & Abakumov, A. M. Implementation of micro-ball nanodiamond anvils for high-pressure studies above 6 Mbar. *Nat. Commun.* **3**, 1163 (2012).
4. Friedrich, A. *et al.* Novel rhenium nitrides. *Phys. Rev. Lett.* **105**, 1–4 (2010).
5. Bykov, M. *et al.* High-Pressure Synthesis of a Nitrogen-Rich Inclusion Compound  $\text{ReN}_8 \cdot x\text{N}_2$  with Conjugated Polymeric Nitrogen Chains. *Angew. Chem., Int. Ed.* **57**, 9048–9053 (2018).
6. Eremets, M. I., Gavriluk, A. G., Trojan, I. A., Dzivenko, D. A. & Boehler, R. Single-bonded cubic form of nitrogen. *Nat. Mater.* **3**, 558–63 (2004).
7. Zhao, Z. *et al.* Nitrogen concentration driving the hardness of rhenium nitrides. *Sci. Rep.* **4**, 4797 (2014).
8. Zhao, E. & Wu, Z. Electronic and mechanical properties of 5d transition metal mononitrides via first principles. *J. Solid State Chem.* **181**, 2814–2827 (2008).
9. Kawamura, F., Yusa, H. & Taniguchi, T. Synthesis of rhenium nitride crystals with  $\text{MoS}_2$  structure. *Appl. Phys. Lett.* **100**, 2–5 (2012).
10. Zhong, Y. *et al.* Transition Metal Carbides and Nitrides in Energy Storage and Conversion. *Adv. Sci.* **3**, 1500286 (2016).
11. Wang, S. M. *et al.* Synthesis, Crystal Structure, and Elastic Properties of Novel Tungsten Nitrides. *Chem. Mater.* **24**, 3023–3028 (2012).
12. Wang, S. *et al.* The Hardest Superconducting Metal Nitride. *Sci. Rep.* **5**, 13733 (2015).
13. Lei, L., Yin, W., Jiang, X., Lin, S. & He, D. Synthetic route to metal nitrides: High-pressure solid-state metathesis reaction. *Inorg. Chem.* **52**, 13356–13362 (2013).
14. Kloß, S. D. & Schnick, W. Nitridophosphates - A Success Story of Nitride Synthesis. *Angew. Chem., Int. Ed.* (2018). doi:10.1002/anie.201812791
15. Jiang, X., Lei, L., Hu, Q., Feng, Z. C. & He, D. High-pressure Raman spectroscopy of  $\text{Re}_3\text{N}$  crystals. *Solid State Commun.* **201**, 107–110 (2015).
16. Schneider, S. B., Frankovsky, R. & Schnick, W. Synthesis of Alkaline Earth Diazenides  $\text{M}_{\text{AE}}\text{N}_2$  ( $\text{M}_{\text{AE}} = \text{Ca}, \text{Sr}, \text{Ba}$ ) by Controlled Thermal Decomposition of Azides under High Pressure. *Inorg. Chem.* **51**, 2366–2373 (2012).
17. Schneider, S. B., Frankovsky, R. & Schnick, W. High-Pressure Synthesis and Characterization of the Alkali Diazenide  $\text{Li}_2\text{N}_2$ . *Angew. Chem., Int. Ed.* **51**, 1873–1875 (2012).
18. Vogel, S., Buda, A. T. & Schnick, W. United in Nitride: The Highly Condensed Boron Phosphorus Nitride  $\text{BP}_3\text{N}_6$ . *Angew. Chem., Int. Ed.* **57**, 13202–13205 (2018).